Received: 18 December 2023 | Revised: 20 January 2025 | Accepted: 20 January 2025
DOI: 10.1002/suco.202301131

ARTICLE

fib CEB·FIP WILEY

Effect of calcined clay reactivity on the risk of restrained shrinkage-induced early-age concrete cracking

Emily Canda[1] | **Quang Dieu Nguyen**[1] | **Rackel San Nicolas**[2] | **Haleh Rasekh**[1] | **Arnaud Castel**[1]

[1]School of Civil and Environmental Engineering, University of Technology Sydney (UTS), Sydney, NSW, Australia
[2]Department of Infrastructure Engineering, University of Melbourne (UoM), Melbourne, VIC, Australia

Correspondence
Quang Dieu Nguyen, School of Civil and Environmental Engineering, University of Technology Sydney (UTS), Sydney, NSW 2007, Australia.
Email: quangdieu.nguyen@uts.edu.au

Funding information
Australian Research Council; Cement Concrete Aggregate Australia

Abstract
A combination of limestone and calcined clay has emerged as a promising supplementary cementitious material due to its abundant availability to replace traditional supplementary cementitious materials such as fly ash or ground-granulated blast-furnace slag in reducing concrete's carbon footprint. Although different properties have been considered, very limited attention was paid to the early-age cracking behavior of limestone calcined clay cement (LC3) concretes. This study aims to investigate the influence of calcined clay reactivity on the early-age cracking potential of LC3 concretes using the restrained ring test. Mechanical properties, time to cracking, tensile creep coefficient, and total shrinkage were measured. Results showed that the reactivity of calcined clay significantly impacted total shrinkage, creep coefficients, and time to cracking. LC3 concretes exhibited higher tensile creep coefficients than pure ordinary Portland cement concrete, which can provide beneficial tensile stress relaxation delaying concrete cracking. An apparent calcined clay reactivity coefficient (R_{app}) was proposed correlating well with the time to cracking of the restrained LC3 concrete rings, thus offering practical guidance for the selection of suitable calcined clays and mix designs for specific high-risk applications.

KEYWORDS
calcined clay reactivity, concrete cracking, LC3, R_{app}, restrained shrinkage, Ring test, tensile creep

1 | INTRODUCTION

The global effort to achieve the net-zero target by 2050 has driven significant focus on the construction materials industry.[1,2] Concrete, being the second-most consumed material worldwide after water, plays a crucial role in this mission.[3,4] However, the decarbonization pathway is facing several challenges due to the intrinsic hard-to-abate feature of concrete.[5] Specifically, carbon dioxide emissions are mostly linked to cement production, which accounts for 5%–8% of anthropogenic CO_2 emissions.[6] To address this, the partial replacement of ordinary Portland cement (OPC) by supplementary cementitious materials (SCMs) has been an effective approach to reducing the carbon footprint of concrete.[7,8] Nonetheless, the future availability of traditional SCMs such as fly ash or ground-granulated blast-furnace slag (GGBFS) is uncertain due to the closure of coal-fired power station or alternative methods such as electrolysis and direct reduced iron in steel production.[9–11]

Calcined clay has gained significant attention, in the past two decade, as an alternative SCM because clay is available in abundant amount worldwide.[12,13] The binder with cement substituted by calcined clay and limestone up to 50 wt.% is denoted as limestone calcined clay cement (LC3), which is demonstrated as an alternative to OPC concrete. Previous studies have reported comparable or superior performance in terms of mechanical and durability properties compared to OPC concretes. For instance, Joseph et al.[14] indicated that LC3 concretes, produced from calcined clay with at least 40 wt.% kaolinite content, could achieve similar 28-day strength as conventional OPC concrete. Extended curing beyond 7 days after casting is not necessary for LC3 concretes, as the predominant microstructure development occurs within the first 7 days.[15] In terms of durability properties, resistivity, absorption rate, and chloride diffusion resistance improved significantly due to pore structure refinement with the presence of calcined clay and limestone in LC3 concrete.[16–18] However, the high replacement levels of calcined clay and limestone cause a lack of calcium hydroxide buffer in the microstructure, reducing the resistance against carbonation.[19] LC3 blends also demonstrated good performance in terms of sulfate expansion and alkali-silica reaction resistance.[20,21]

Concrete cracking potential is a crucial factor that significantly affects both the structural and durability properties. Cracking occurs when tensile stress exceeds the tensile strength within a concrete element.[22,23] It can lead to reduced load-bearing capacity or accelerated deterioration of reinforced concrete structures, as it provides a pathway for aggressive ions to reach the steel-concrete interface.[24] Shrinkage, an inevitable process in cementitious materials, is one of the major causes of concrete cracking. Concrete cracking potential induced by shrinkage also depends on several factors, including tensile strength, elastic modulus, tensile creep coefficient, degree of restraint, and increasing rate of tensile stress development.[25,26] For example, higher tensile strength and tensile creep coefficient can delay the cracking time while higher shrinkage and degree of restraint can increase the risk of early-age cracking and shorten the cracking time. Therefore, studies on shrinkage-induced concrete cracking have been conducted for both conventional and blended SCM concretes. Miltenberger et al.[27] and See et al.[28] demonstrated that using shrinkage-reducing admixtures could effectively decrease the cracking potential of concrete. Fly ash has been found to reduce shrinkage and increase relaxation, resulting in enhanced cracking resistance of fly ash blended concrete.[29] Similarly, the improved cracking resistance of fly ash concrete was also reported in other studies.[30,31] On the other hand, GGBFS reduced the cracking resistance of blended cement concretes for compressive strength less than 40 MPa while GGBFS concrete presented a similar cracking potential to 100 wt.% OPC concrete for compressive strength higher than 50 MPa.[31] This was attributed to the different instantaneous stress rate development in low and high strength grades concretes with high slag content.[31]

The early-age cracking potential of LC3 concretes was investigated in few studies. Ston and Scrivener reported lower basic creep compliance compared to reference OPC concrete when subjected to a 10%–15% stress level of 28-day strength.[32] Scrivener et al.[33] reported a similar autogenous shrinkage while higher autogenous shrinkage of LC3 pastes than that of OPC paste was exhibited in other studies.[34,35] Total shrinkage was found to be similar between LC3 and OPC concretes.[22,36] Afroz et al.[37] identified that the risk of early-age cracking of LC3 concrete was high based on their shorter cracking time compared to 100 wt.% OPC reference mix. The greater risk of early-age cracking of LC3 concretes, and mortars in Sumaiya's study was attributed to the higher total shrinkage rate/autogenous shrinkage rate ratio of LC3 blends. However, only one type of calcined clay was used.[37]

This study aims to investigate the influence of calcined clay reactivity on early-age cracking of LC3 concretes. Two calcined clays were used (low and high reactivity). Different replacement contents of calcined clay and limestone in the binder were considered. Several properties influencing the performance of LC3 concrete cracking including compressive strength, tensile strength, elastic modulus, total shrinkage, tensile stress, and creep coefficient were evaluated and compared to reference concretes including OPC and blended cement (with fly ash and GGBFS) concretes. Furthermore, correlations between calcined clay reactivity and properties related to the risk of early-age cracking are explored in this study.

2 | MATERIALS AND MIX DESIGNS

2.1 | Materials

To investigate the influence of clay reactivity on the risk of early-age cracking, two calcined clays denoted as calcined clay 1 and calcined clay 2 (CC1 and CC2) were used in this study. The kaolinite content of the raw clays was unknown to the authors because these calcined clays were received as commercial products. Instead, the amorphous content (wt.%) in the two calcined clays was measured by X-ray diffraction (XRD) and considered governing the reactivity of the calcined clays. A random powder specimen was prepared by back loading method and a known quantity of crystalline silicon was added to determine the amorphous proportion. XRD measurement was conducted by PANalytical X'Pert PRO XRD system with 45 kV and 40 mA, scan range from 5° to 70° and 0.013° 2θ step size. Data collected were processed by High Score Plus software using PDF 4+ databased followed by Rietveld refinement to quantify the crystalline phases and the amorphous fraction.[38,39] After the measurement, the amorphous content in CC1 and CC2 is 79 wt.% and 51 wt.%, respectively. The details of the XRD-Rietveld analysis of the two calcined clays are presented in Table 1. Moreover, the XRD-Rietveld pattern of calcined clay 1 is presented in Figure 1. Based on the amorphous content, which is considered as a suitable clay reactivity indicator, CC1 and CC2 were categorized as medium-grade and low-grade calcined clay, respectively. General purpose (GP) cement (Australian Standard AS 3792[40]) was used in this study. Limestone was supplied by Omya Australia compliant with ASTM C595.[41] The chemical composition of all materials determined by X-ray fluorescence and particle size distribution determined by laser diffraction are presented in Table 2 and Figure 2, respectively. The coarse aggregate was Basalt with a maximum nominal size of 10 mm and a specific gravity of 2.8. Sydney sand was used as fine aggregate in this study with water absorption of 3.5% and specific gravity of 2.65. The gradation of aggregates was presented in a previous study by the authors.[31]

TABLE 1 X-ray diffraction-Rietveld results of the two calcined clays.

	Calcined clay 1	Calcined clay 2
Quartz (SiO_2)	2.0 ± 0.1	49.1 ± 0.1
Mullite ($Al(Al_{1.272}Si_{0.728}O_{4.864})$)	6.4 ± 0.1	–
Dickite ($Al_2Si_2O_5(OH)_4$)	7.3 ± 0.1	–
Kaolinite ($Al_2Si_2O_5(OH)_4$)	4.1 ± 0.1	–
Anatase (TiO_2)	1.5 ± 0.1	–
Amorphous	78.8 ± 0.1	50.9 ± 0.1

2.2 | Mix designs

Four concrete mix compositions were created with one reference mix containing only GP cement and three blended cement mixes with calcined clays (LC3 mixes). The replacement percentage of LC3 mixes ranged from 30 to 44 wt.%. Due to the high reactivity of calcined clay CC1, only a replacement rate of 44 wt.% was considered. All concrete mixes were designed to achieve a concrete grade between 32 and 40 MPa at 28 days. Consequently, the water/binder ratios were modified according to the different calcined clay reactivity and replacement rates while keeping a constant total binder mass. The mass ratio of calcined clay: limestone in all LC3 mixes was approximately 2:1. The aggregates were in saturated surface dry condition prior to the mixing, and a vibration table was used for concrete compaction. The superplasticizer was added to obtain acceptable workability for all mixes. Based on the cracking time of restrained rings

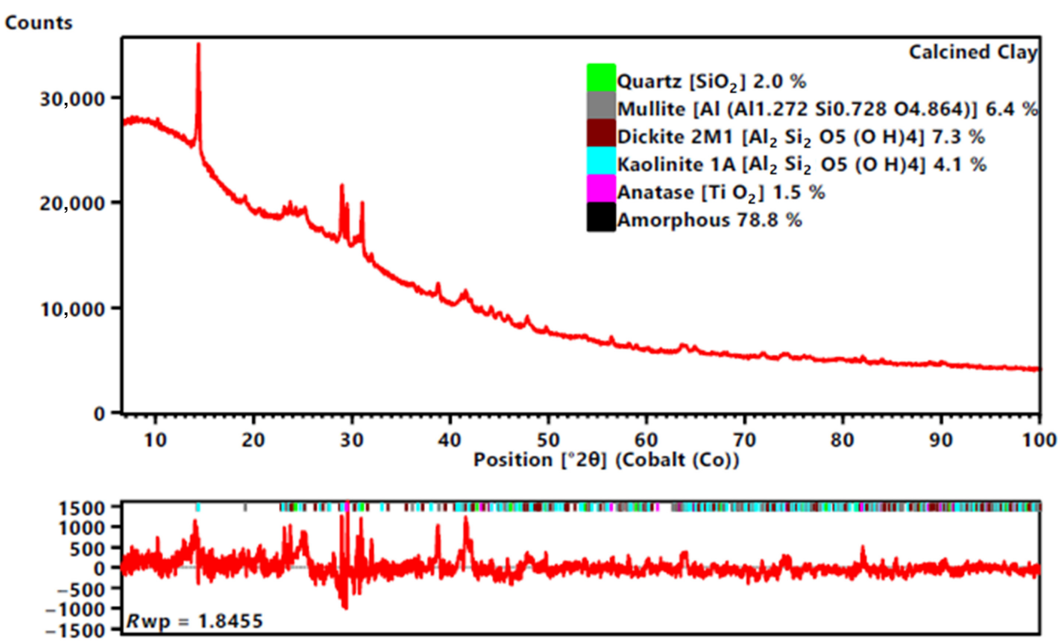

FIGURE 1 X-ray diffraction-rietveld patterns of calcined clay 1.

TABLE 2 Chemical compositions of binder constituents.

Wt. %	SiO_2	Al_2O_3	Fe_2O_3	CaO	MgO	Na_2O	K_2O	TiO_2	SO_3	LOI
GP cement	18.96	4.81	3.14	63.76	1.20	0.21	0.46	0.22	2.37	3.96
CC1	51.22	39.37	2.56	0.18	0.10	0.20	0.09	2.88	0.02	2.19
CC2	70.42	22.34	2.34	0.49	0.16	0.10	0.19	1.10	0.02	1.76
Limestone	1.10	0.24	0.17	54.84	1.53	–	–	–	0.03	43.11

Abbreviations: CC1, calcined clay 1; CC2, calcined clay 2; GP, general purpose; LOI, loss on ignition.

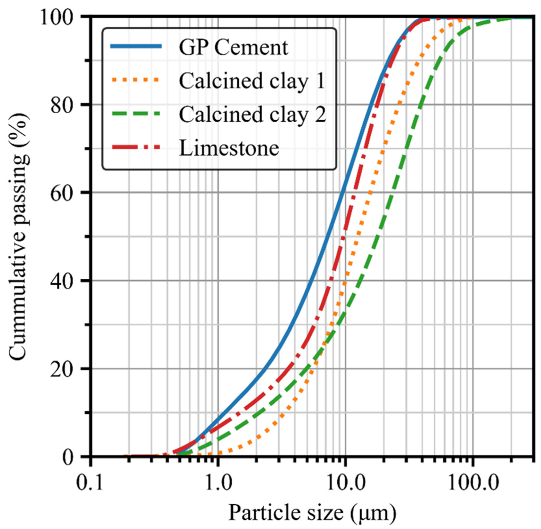

FIGURE 2 Particle size distribution of general purpose (GP) cement, calcined clays, and limestone.

(Section 4.2), the effects of superplasticizers on shrinkage and cracking time could be disregarded as all mixes cracked after 5 days. The concrete casting was conducted in a controlled room at a temperature of 23°C and concrete specimens were demoulded 1 day after batching. Table 3 shows the details of the concrete mixes with aggregate mass in saturated surface dry condition and the average 28-day compressive strength obtained under standard wet curing condition ($f_{cm,28}$) compliant with Australian Standard AS 1012.8.4 and ASTM C192.[42,43]

3 | METHODOLOGY

3.1 | Time-dependent mechanical properties and total shrinkage

Mechanical properties relevant to the risk of early-age cracking, including indirect tensile strength (Brazil test) and elastic modulus, were measured in accordance with ASTM C496 and C469,[44,45] respectively, using standards cylinders 100 × 200 mm. The cylinders were cured at ambient conditions in a controlled room with 23 ± 2°C and 50 ± 3% relative humidity (RH) to match the testing condition of shrinkage and tensile creep experiments. The mechanical properties were tested at 1, 2, 3, 7, and 28 days after casting. The total shrinkage was determined by using concrete prisms of 75 × 75 × 280 mm for up to 28 days. Twenty-four hours after casting, the prisms were demoulded, and initial shrinkage value was measured within 5 min after demoulding. The subsequent shrinkage values were monitored with a vertical comparator in a controlled room at a temperature of 23 ± 2°C and RH of 50 ± 3%.[46] All mechanical properties and shrinkage were determined in triplicate and the average values were reported in this study.

3.2 | Concrete restrained and unrestrained ring test

The concrete ring test was modified from ASTM C1581[47] and was used in previous studies by the authors.[25,31,48,49] Two types of concrete rings were fabricated: restrained ring and unrestrained ring. All ring specimens, except for LC3-CC2-44, were demoulded after 1 day of casting. Ring specimens of LC3-CC2-44 mix design were demoulded after 2 days due to their low tensile strength, which significantly increased the risk of cracking during demoulding process. The concrete rings inner diameter is 260 mm, outer diameter of 340 mm, height of 70 mm and thickness of 35 mm. The restrained concrete ring was cast with a steel ring on inner surface to evaluate the risk of early-age cracking induced by restrained shrinkage. For unrestrained rings, the inner steel mold was removed during the demoulding process. Unrestrained concrete rings without the steel ring were used to monitor the total shrinkage in unrestrained conditions compared to restrained rings with inner steel ring. The inner surface of unrestrained rings was covered with waterproof aluminum foil to maintain the same drying condition as restrained condition. Three strain gauges were attached at mid-height of the inner surface in each ring specimen and were connected to a data acquisition system to record the strain values up to 28 days. The strain measurement of both restrained and unrestrained steel rings

TABLE 3 Concrete mixtures details.

Materials (kg/m³)	Ref	LC3-CC1-44	LC3-CC2-30	LC3-CC2-44
Coarse aggregate	1043	1010	1053	1092
Fine aggregate	853	827	862	893
GP cement	360	201.6	252	201.6
Calcined clay 1	–	108	–	–
Calcined clay 2	–	–	72	110.2
Limestone	–	50.4	36	48.2
Water	176.4	176.4	144	115.2
Total binder	360	360	360	360
Binder replacement (%)	0	44	30	44
Water/binder ratio	0.49	0.49	0.40	0.32
$f_{cm,28}$ (MPa)	32.5 ± 0.6	39.6 ± 0.4	37.8 ± 1.5	37.0 ± 0.9

Abbreviations: CC1, calcined clay 1; CC2, calcined clay 2; GP, general purpose; LC3, limestone calcined clay cement.

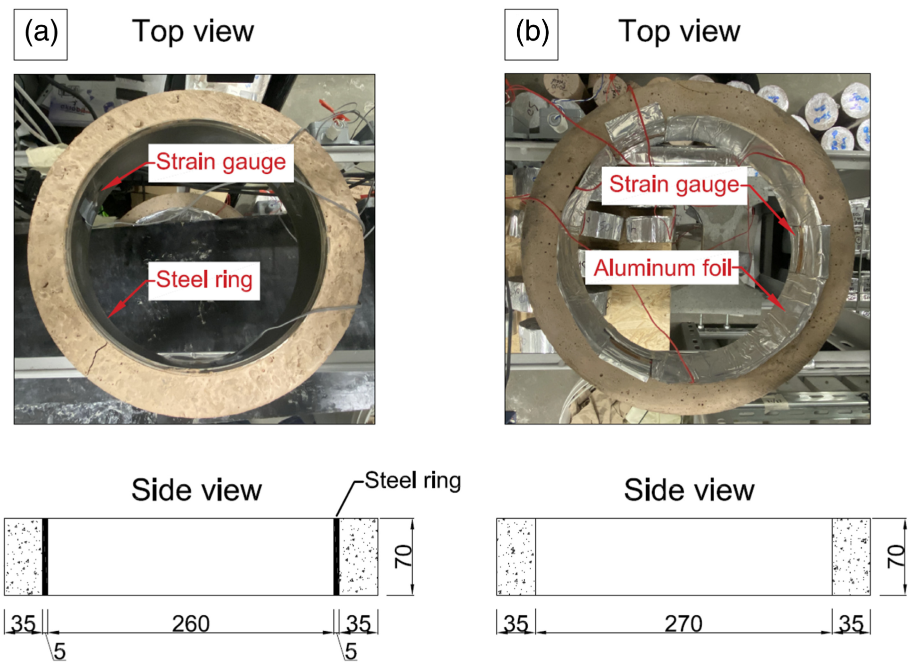

FIGURE 3 Details of (a) restrained rings, and (b) unrestrained rings in mm.

started after demoulding. The details of the restrained and unrestrained ring are shown in Figure 3. Two restrained rings and two unrestrained rings were fabricated for each mix design. Except for the inner surface, all other surfaces of the restrained and unrestrained rings were exposed to drying at a temperature of 23 ± 2°C and a RH of 50 ± 3%.

3.3 | Early-age tensile creep by dog-bone specimens

A dog-bone-shaped specimen under uniaxial tensile load was utilized to measure the tensile creep.[25,31,48–50] The specimen length is 300 mm, biggest width of 200 mm, smallest width of 70 mm and thickness of 35 mm. The coarse aggregate size of 10 mm is lower than size limit of 13 mm in ASTM C1581[47] which using the similar specimen's thickness. The detailed dimensions of the dog-bone specimens are presented in Figure 4a. The specimens were connected to the creep rig using embedded threaded bolts and steel plates at each end. Two strain gauges were attached at the middle of each specimen and connected to the data acquisition system. The homogeneity of specimens was validated by the consistent strain data between two strain gauges. The creep rig test arrangement is shown in Figure 4b. The dog-bone specimens were loaded in the creep rig after 2 days of casting with the

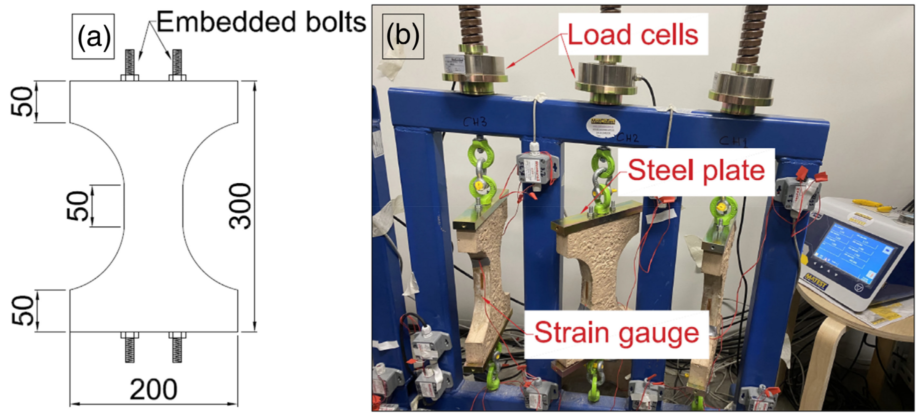

FIGURE 4 (a) Details of a dog-bone specimen and (b) tensile creep test set-up.

sustained loading at 50% of the 2-day tensile strength measured by indirect (splitting) tensile test ASTM C496.[45] To be specific, the loading rate of Ref, LC3-CC1-44, LC3-CC2-30, and LC3-CC2-44 was 2.82, 1.87, 1.62, and 1.64 kN, respectively. The identical dog-bone-shaped specimens without loading, that is, free dog-bone specimens were used to monitor shrinkage and calculate the creep coefficient. The early-age tensile creep coefficient was determined by using loaded dog-bone specimens and companion free dog-bone specimens. The strain measurement in loaded and unloaded dog-bone specimens was the average of three replicates. The total strain ($\varepsilon_{\text{total}}(t)$) at time t measured on loaded dog-bone specimens is the combination of three components as follows:

$$\varepsilon_{\text{total}}(t) = \varepsilon_{\text{e}}(t_0) + \varepsilon_{\text{sh}}(t) + \varepsilon_{\text{cp}}(t). \quad (1)$$

where $\varepsilon_{\text{e}}(t_0)$ is the elastic concrete strain measured at the initial loading time (Day 2 in this study), $\varepsilon_{\text{sh}}(t)$ is the shrinkage strain measured on the free dog-bone specimens and $\varepsilon_{\text{cp}}(t)$ is the tensile creep strain of the loaded dog-bone specimens. The tensile creep coefficient ($\varphi(t,t_0)$), depending on concrete age (t) and initial loading time ($t_0 = 2$), is calculated based on Equation (2):

$$\varphi(t,2) = \frac{\varepsilon_{\text{cp}}(t)}{\varepsilon_{\text{e}}(2)} = \frac{\varepsilon_{\text{total}}(t) - \varepsilon_{\text{e}}(2) - \varepsilon_{\text{sh}}(t)}{\varepsilon_{\text{e}}(2)}. \quad (2)$$

4 | RESULTS AND DISCUSSION

4.1 | Time-dependent mechanical properties and total prism shrinkage

Figure 5 presents the mechanical properties of concretes, including indirect tensile strength (a) and modulus of elasticity (b) up to 28 days after casting. In order to provide a comprehensive comparison between different SCMs, three additional blended cement concretes from a previous study by the authors were included in Figure 5.[25] These concretes, containing 30% fly ash, 40% GGBFS, and 60% GGBFS, denoted as FA concrete, slag concrete 40%, and slag concrete 60% in Figure 5, respectively, achieving the same concrete grade of 32 MPa.[25] LC3-CC2-44 exhibited the lowest indirect tensile strength at 1 day after casting (Figure 5a). This can be attributed to the lower reactivity and high replacement level of CC2. In contrast, the 1-day indirect tensile strength of LC3-CC2-30 (with a lower replacement rate) and LC3-CC1-44 (with higher clay reactivity) were higher than LC3-CC2-44 and the concrete containing 60% GGBFS. The Ref concrete displayed the highest 1-day indirect tensile strength of approximately 1.8 MPa. From Day 2 to Day 7, LC3-CC2-30 and LC3-CC2-44 demonstrated a similar indirect tensile strength while LC3-CC1-44 had the highest indirect tensile strength among three LC3 concretes. The Ref concrete obtained the highest indirect tensile strength in the first 7 days. The development rate of the indirect tensile strength in LC3 concretes was higher than that of reference concrete (100% GP cement) from 7 to 28 days. Noticeably, at 28 days, LC3-CC2-30 concrete showed the highest indirect tensile strength among all concretes which can be attribute to the pozzolanic reactions and reaction between calcined clay and limestone at 30% replacement rate, outperforming the reference concrete.[17,51] The three LC3 concretes exhibited a lower elastic modulus at Day 1 compared to the reference and other blended cement concretes (Figure 5b). Among the three LC3 concretes, LC3-CC1-44 showed the highest 1-day and 2-day elastic modulus while LC3-CC2-30 presented the highest elastic modulus from Day 3 to Day 28. The Ref concrete had the highest modulus of elasticity among all concretes over the whole test duration, except for Day 1. LC3-CC2-30 had the highest elastic modulus increasing rate from Day 1 to Day 28 while LC3-CC1-44 concrete showed the lowest rate.

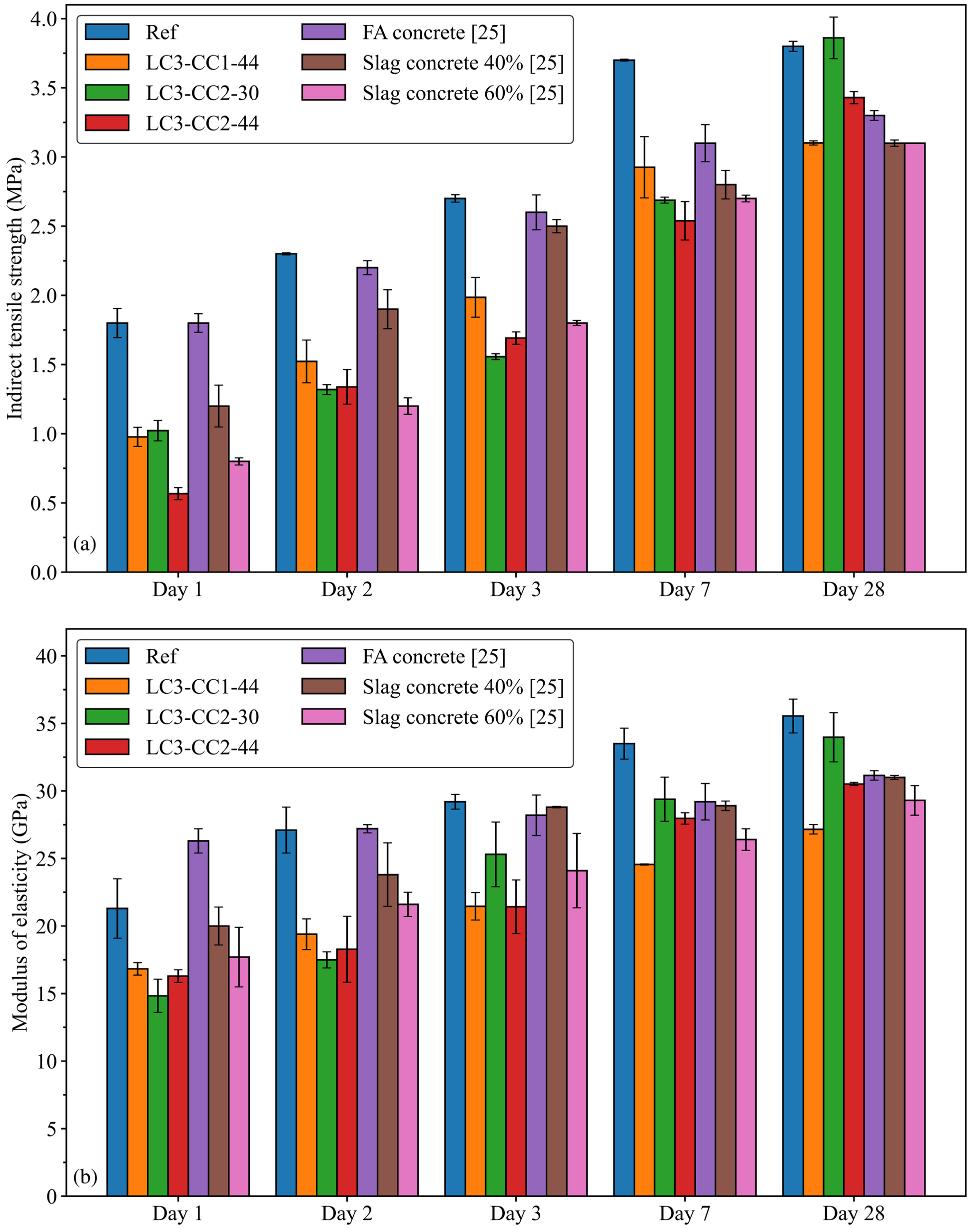

FIGURE 5 Time-dependent mechanical properties on dry curing condition: (a) indirect tensile strength and (b) modulus of elasticity. CC1, calcined clay 1; CC2, calcined clay 2; LC3, limestone calcined clay cement.

The total shrinkage of the concrete prisms up to 28 days is shown in Figure 6a and the development of total shrinkage over the first 7 days is shown in Figure 6b. The type of SCM and the replacement rate significantly influenced the development of the total shrinkage. Specifically, 3 days after casting, concrete with 40% GGBFS, fly ash concrete, LC3-CC1-44, and LC3-CC2-30 showed a lower shrinkage compared to Ref concrete. The 6-day total shrinkage value was similar among LC3-CC2-30, LC3-C2-44, and concrete with 40% GGBFS at a value of −190 μm/m. From Day 6 to Day 14, only the fly ash concrete displayed smaller shrinkage values than the reference concrete. From Day 7 to Day 28, the increasing shrinkage rate of LC3-CC2-44 concrete was slow, leading to the lowest total shrinkage value of −330 μm/m among the LC3 concretes at 28 days. The LC3-CC1-44 concrete exhibited the highest total shrinkage value among all concretes from 4 days of casting, reaching a 28-day total shrinkage value of approximately −550 μm/m. The high shrinkage of LC3-CC1-44 can be attributed to the high reactivity of calcined clay 1. The LC3-CC1-44 shrinkage may be decreased by utilizing a longer curing duration, as suggested by Li et al.[52] LC3-CC2-30 concrete demonstrated higher total shrinkage from Day 7 to Day 14 compared to 40% GGBFS, followed by a similar shrinkage development trend as the concrete with 40% GGBFS, with a shrinkage value of −400 μm/m at 28 days. Comparing LC3-CC1-44 and LC3-CC2-44 concretes, which had the same replacement rate of 44% for calcined clay and limestone, the higher reactivity of CC1 resulted in a significantly higher total

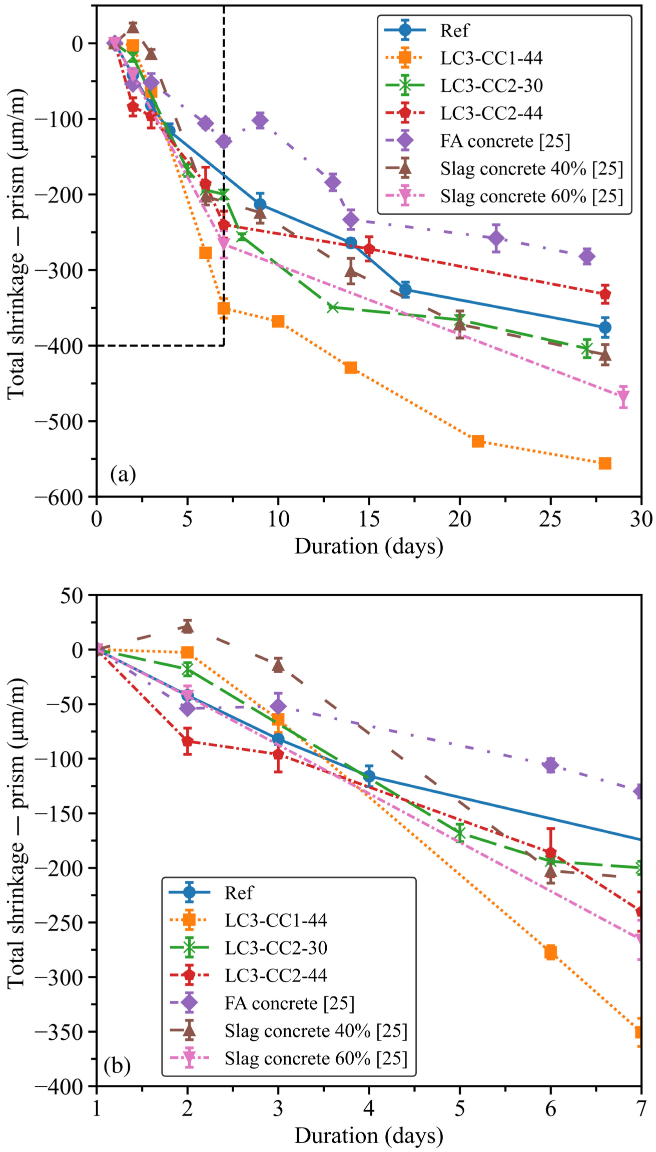

FIGURE 6 (a) Total prism shrinkage up to 28 days after casting and (b) zoomed total prism shrinkage up to 7 days after casting. CC1, calcined clay 1; CC2, calcined clay 2; LC3, limestone calcined clay cement.

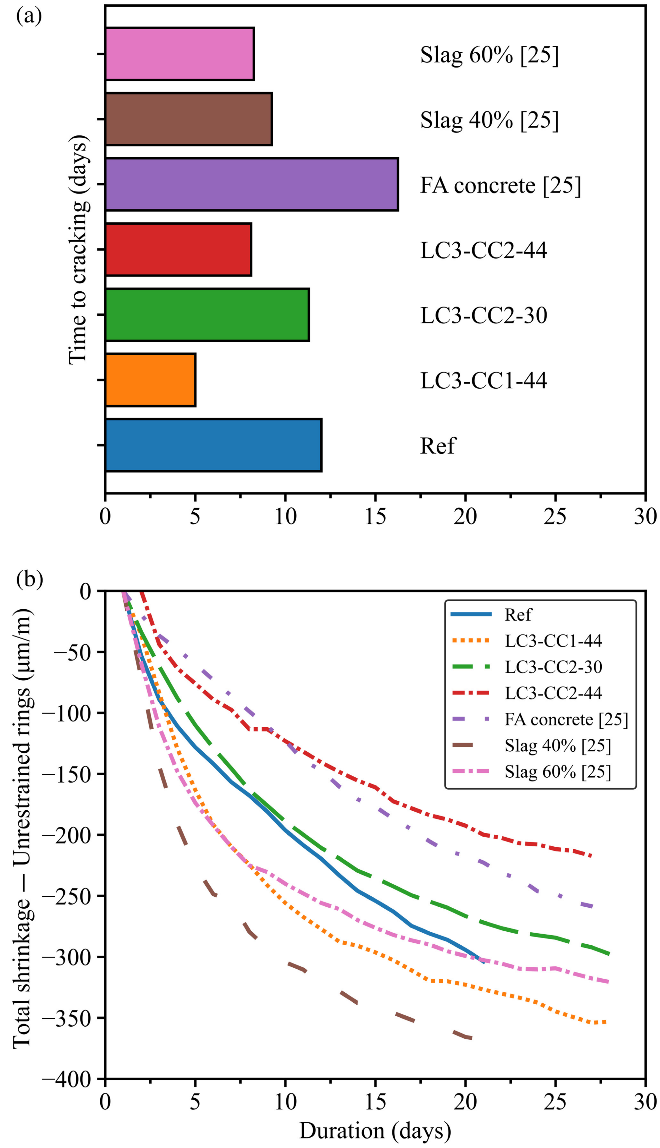

FIGURE 7 (a) Cracking time in days of restrained rings and (b) total shrinkage of unrestrained rings. CC1, calcined clay 1; CC2, calcined clay 2; LC3, limestone calcined clay cement.

shrinkage of approximately −220 μm/m at 28 days compared to LC3-CC2-44, despite LC3-CC2-44 concrete having a lower water/binder ratio (Table 2). The higher reactivity of CC1 may result in higher hydration degree and higher autogenous shrinkage in LC3-CC1-44 concrete.[22,53] This highlights the important effect of the calcined clay reactivity on the total shrinkage development of LC3 concretes.

4.2 | Time to cracking in concrete rings

Figure 7a presents the restrained shrinkage-induced time to cracking in the restrained rings, and Figure 7b shows the total shrinkage of the unrestrained rings. Although two restrained rings were used to monitor the cracking time, time to cracking was determined conservatively as the first observed crack in the restrained ring was recorded as a sudden drop in steel strain by the datalogger.[31] The reference concrete (100% GP cement) cracked after 12 days of casting. Fly ash concrete exhibited the longest cracking time at 16.25 days while LC3-CC1-44 concrete displayed the shortest cracking time at 5 days. The high total shrinkage observed in LC3-CC1-44 (Figure 6) can account for its short cracking time in comparison with other 32 MPa grade concretes. In contrast, the use of CC2 (low reactivity) instead of CC1 (high reactivity) significantly increased the cracking time. Specifically, LC3-CC2-44 extended the time to cracking to 8 days, which is similar to the cracking time of concrete containing 40% or 60% GGBFS. In addition, by reducing the proportion of CC2 and limestone in the binder from 44 to 30 wt.%, the cracking time of LC3-CC2-30 increased to 11.5 days, comparable to the cracking time of Ref concrete (12 days). This result indicates that different calcined clays with varying reactivity can significantly impact the shrinkage-induced cracking time, and LC3 concretes can obtain comparable cracking time to conventional concrete (100% GP cement) or other blended concrete with GGBFS, for example, by using CC2 in this study.

The total shrinkage of the unrestrained concrete rings is shown in Figure 7b. LC3-CC2-44 exhibited the lowest total shrinkage, approximately −210 μm/m, up to 28 days. This can be attributed to the total shrinkage of LC3-CC2-44 being recorded from Day 2 instead of Day 1 in other mixes. Among the three LC3 concretes, LC3-CC1-44, with highly reactive CC1 calcined clay, obtained the highest total shrinkage at −350 μm/m at 28 days. This result is consistent with the results of total shrinkage obtained with the standard concrete prisms. The high total shrinkage of LC3-CC1-44 unrestrained rings can lead to the shortest cracking time at 5 days in restrained rings. However, GGBFS concrete with 40% replacement obtained the highest total shrinkage in unrestrained rings while exhibiting a time to cracking at 9.25 days. This result reveals that the cracking time is dependent on several factors in addition to total shrinkage, which is thoroughly discussed in the following sections.

The concrete tensile stress ($\sigma_{c,act}$) in the restrained rings can be calculated from the measured steel strain,[25] ε_{st} in Equation (3), as follows:

$$\sigma_{c,act}(\mathrm{MPa}) = -\varepsilon_{st} \times E_{st} \times \frac{R_{OS}^2 - R_{IS}^2}{2R_{OS}^2} \times \frac{R_{OC}^2 + R_{OS}^2}{R_{OC}^2 - R_{OS}^2}. \qquad (3)$$

where E_{st} is the steel ring elastic modulus (200 GPa), R_{OS} is the outer radius of the steel ring (135 mm), R_{IS} is the inner radius of the steel ring (130 mm), and R_{OC} is the outer radius of the concrete ring (170 mm).

Furthermore, the early-age cracking potential can be also evaluated from the instantaneous stress rate (S) from the development rate of steel strain[31,47] as presented in Equation (4):

$$S\,(\mathrm{MPa/day}) = \frac{G \times |\alpha_{avg}|}{2\sqrt{t}}. \qquad (4)$$

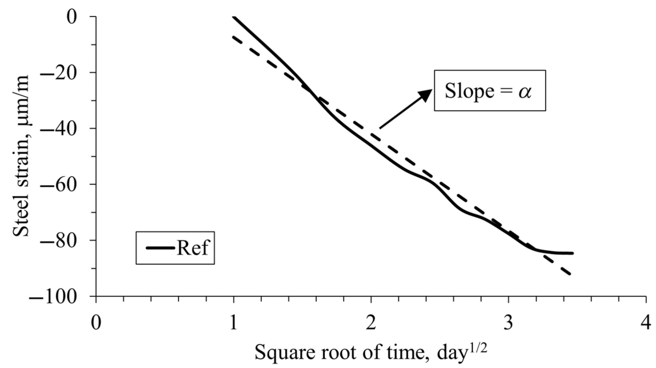

FIGURE 8 An example of average strain rate calculation of Ref concrete.

where α_{avg} is the average strain rate development factor against the square root of duration ([m/m]/days$^{1/2}$).[31] An example of average strain rate calculation of Ref concrete is presented in Figure 8. t is the elapsed time at cracking (days) and G is the ring dimensions and steel ring elastic modulus, which is calculated as follows:

$$G\,(\mathrm{GPa}) = \frac{E_{st} \times R_{IC} \times h_{st}}{R_{IS} \times h_c} \qquad (5)$$

where $E_{st} = 200$ GPa, R_{IC} is the inner radius of concrete ring ($R_{IC} = R_{OS} = 135$ mm), $R_{IS} = 130$ mm, h_{st} is the thickness of steel (5 mm), and h_c is the thickness of concrete ring (35 mm).

The concrete tensile stress ($\sigma_{c,act}$) and the instantaneous stress rate (S) plotted against the square root of duration are presented in Figure 9a,b, respectively. In Figure 9a, a sudden drop was noticed in all concrete mixes except for fly ash concrete, where a microcrack was observed in fly ash concrete rings at 16.25 days instead of brittle cracking. An example of microcrack and brittle crack is presented in Figure 10a,b, respectively. LC3-CC2-30 concrete showed the highest tensile stress ($\sigma_{c,act}$) values at cracking while LC3-CC1-44 presented the lowest tensile stress at around 3 and 1.7 MPa, respectively. LC3-CC2-44 showed similar $\sigma_{c,act}$ values at cracking to that of concrete containing 40% GGBFS. Generally, except for LC3-CC1-44, the cracking of the restrained rings occurred when $\sigma_{c,act}$ values were higher than 2.2 MPa. This can be attributed to the longer time to cracking (after 8 days), which allowed the concrete to develop tensile strength (f_t) and resist cracking caused by the tensile stress ($\sigma_{c,act}$) development due to restrained shrinkage. In Figure 9b, the cracking potential classifications (low, moderate-low, moderate-high, and high) based on instantaneous stress rate (S) are included according to ASTM C1518.[47] The instantaneous stress

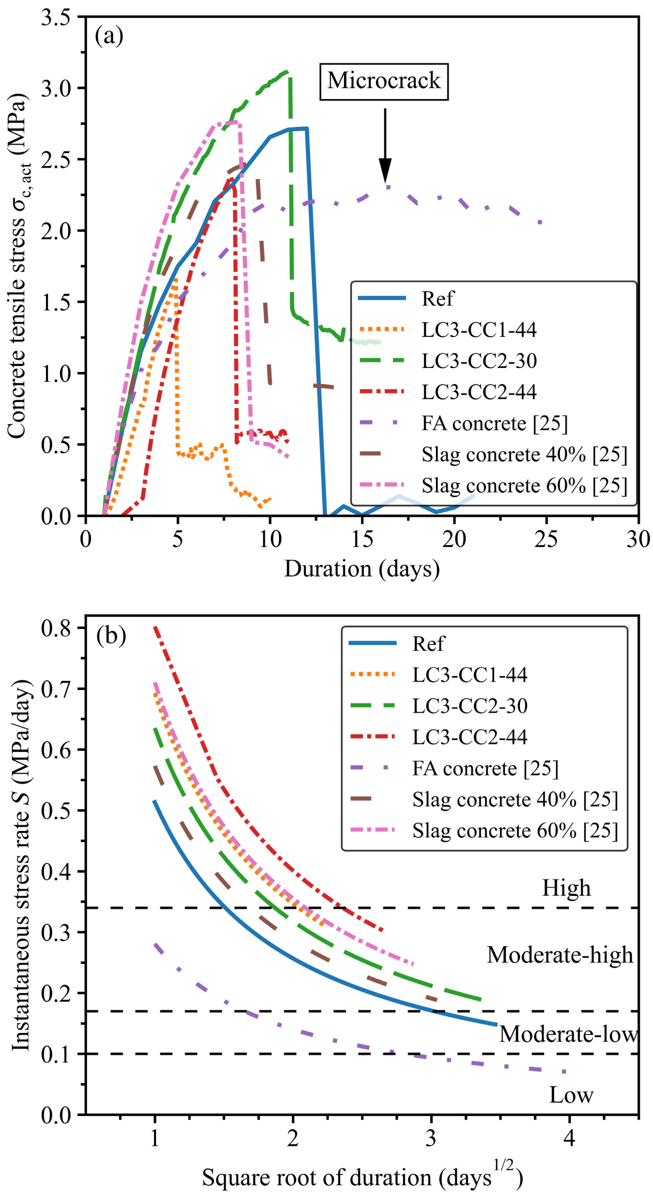

FIGURE 9 (a) Concrete tensile stress and (b) instantaneous stress rate.CC1, calcined clay 1; CC2, calcined clay 2; LC3, limestone calcined clay cement.

rate is presented from the starting of drying (Day 1 or Day 2 for LC3-CC2-44) until the concrete cracking occurred versus square root of duration (day$^{1/2}$). As the drying duration increased, the S values continuously decreased. At cracking, the *S* values were in "low" category for fly ash concrete, "moderate-low" for Ref concrete (100% GP cement), and "moderate-high" for others including LC3 and GGBFS concretes. Noticeably, LC3-CC2-30 exhibited comparable *S* value to Ref at cracking time, with values of 0.18 and 0.14 MPa/day, indicating similar performance in resisting the restrained shrinkage-induced cracking. The development of the instantaneous stress rate of LC3-CC1-44 was equivalent to that of the concrete with 60% GGBFS.

4.3 | Early-age tensile creep

The tensile creep coefficient (φ) of all mixes up to 28 days is shown in Figure 11. The development of the tensile creep coefficients strongly was influenced by the types of SCMs and the binder replacement rates. The variation in creep coefficients based on the different types of SCMs was indicated in a previous study.[54,55] A higher creep coefficient can have positive effects by reducing the concrete tensile stress caused by shrinkage under restrained condition.[56] All LC3 concretes presented a higher tensile creep coefficient than that of Ref concrete up to 10 days after casting. The creep coefficient of LC3-CC1-44, LC3-CC2-30, and LC3-CC2-44 at 10 days was 0.93, 1.52, and 1.55, respectively. From 10 to 28 days, LC3-CC1-44 exhibited a slower increase in creep coefficient compared to GP cement concrete (Ref). The φ values of LC3-CC1-44 and Ref concretes at 28 days were 1.25 and 1.82, respectively. The creep coefficients of reference GP cement concretes were within the range between 1 and 2 of CEM I concrete.[57] LC3-CC2-44 concrete displayed the highest creep coefficient among all concrete mixes until Day 10. Subsequently, the creep coefficient values of LC3-CC2-30 surpassed those of LC3-CC2-44, becoming the highest creep coefficient with an φ value of 2.18 at 28 days, approximately 20% higher than the φ value of Ref concrete. At cracking time of the restrained concrete ring, the φ value of LC3-CC2-30 was approximately 48% higher than that of the Ref concrete. LC3-CC2-44 had a similar creep coefficient value to Ref concrete from 15 to 28 days. Among the blended concretes with SCMs, LC3-CC1-44 had higher φ values than fly ash concrete and 60% GGBFS concrete for up to 14 days. From 14 to 28 days, fly ash concrete demonstrated higher φ values compared to LC3-CC1-44 and 60% GGBFS concrete. Concrete with 60% GGBFS exhibited the lowest creep coefficient over the test duration, which is consistent with the creep coefficient of high slag concrete (CEM III/B) reported in a previous study by Li et al.[57] In addition, LC3-CC2-44 showed a higher creep coefficient than 40% GGBFS concrete until 25 days of casting.

4.4 | Analytical model for the development of concrete tensile stress in restrained rings

An analytical model was proposed to predict the developments of concrete tensile stress in restrained rings in a

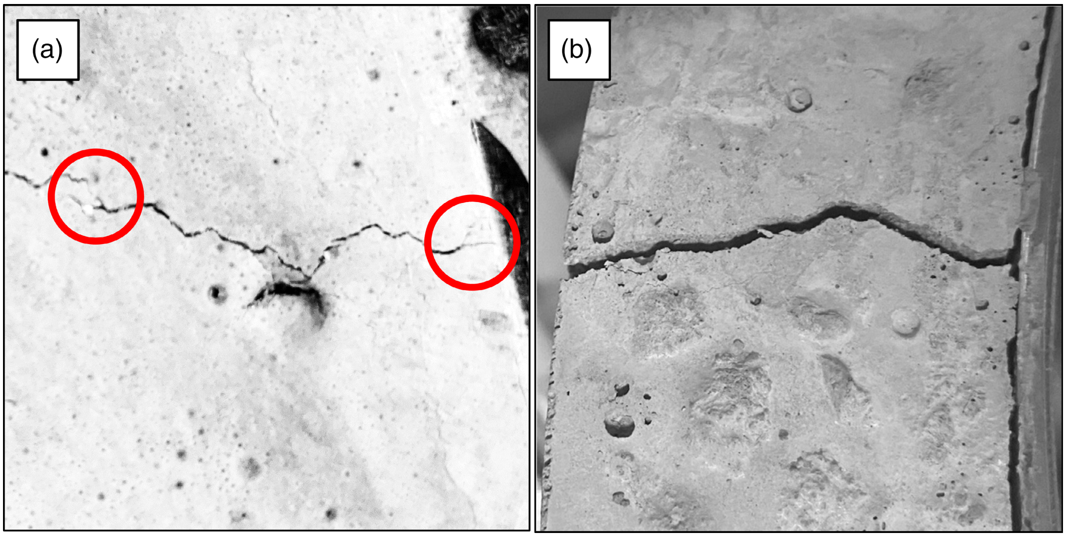

FIGURE 10 (a) Microcracks in red circles and (b) brittle crack.

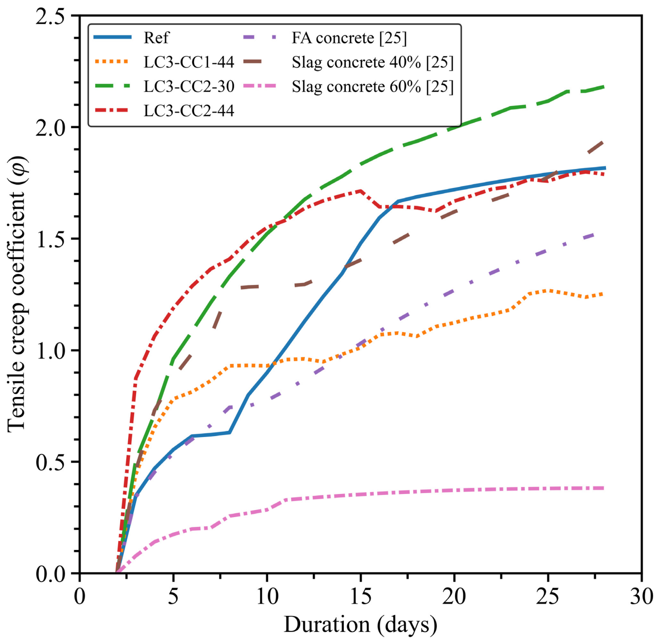

FIGURE 11 Tensile creep coefficients up to 28 days. CC1, calcined clay 1; CC2, calcined clay 2; LC3, limestone calcined clay cement.

previous study.[25] The model offers several advantages as it can effectively consider the influence of factors such as restrained shrinkage, modulus of elasticity, tensile creep, and aging coefficient of concrete on early-age cracking. Furthermore, the validity of this model was verified using a large dataset of 21 concrete mixes including different SCMs such as fly ash and GGBFS, through both experimental results and finite element simulations.[25] The model can be represented by the following Equation (6):

$$\sigma_{c,\text{analytical}}(t)\ (\text{MPa}) = D_R(t) \times \varepsilon_{sh}(t) \times \overline{E}_e(t) \tag{6}$$

where $\sigma_{c,\text{analytical}}(t)$ is the concrete tensile stress at time t calculated by the analytical model, $D_R(t)$ is the degree of restraint at time t (Equation 7), $\varepsilon_{sh}(t)$ is the concrete-free shrinkage at time t. The free shrinkage measured using standard concrete prisms is assigned as $\varepsilon_{sh}(t)$ for simplicity, as concrete rings and standard concrete prisms have a similar hypothetical thickness, that is, volume-to-surface area. $\overline{E}_e(t)$ is the age-adjusted effective modulus[58] at time t as presented in Equation (8):

$$D_R(t) = \frac{1}{\frac{\overline{E}_e(t)}{E_{st}} \times \frac{\left[(1+\upsilon_s)R_{IS}^2 + (1-\upsilon_s)R_{OS}^2\right]}{R_{OS}^2 - R_{IS}^2} + \frac{\left[(1+\upsilon_c)R_{OC}^2 + (1-\upsilon_c)R_{OS}^2\right]}{R_{OC}^2 - R_{OS}^2}} \times \frac{R_{OC}^2 + R_{OS}^2}{R_{OC}^2 - R_{OS}^2} \tag{7}$$

$$\overline{E}_e(t) = \frac{E_c(t)}{1 + \chi(t,t_0) \times \varphi(t,t_0)} \tag{8}$$

where ν_s and ν_c are the Poisson's ratio of steel and concrete, respectively, in this study $\nu_s = 0.3$ and $\nu_s = 0.18$. $\chi(t,t_0) = 0.8$ is the recommended aging coefficient for the relaxation problem of concrete loaded at less than 20 days of age.[56] The aging coefficient value of 0.8 was successfully utilized to predict the degree of restraint and early-age cracking time of OPC concretes and blended cement concretes containing fly ash and GGBFS.[25,50,56]

In addition, the creep coefficient of a concrete specimen depends on the geometry, concrete age (t) and initial loading time (t_0). To take into account these differences, the creep coefficient of dog-bone specimens is converted to that of the concrete rings in Equation (9) as follow:

$$\varphi(t,1)_{\mathrm{r}} = \varphi(t,2)_{\mathrm{d}} \times \frac{(k_2 \times k_3)_{\mathrm{r}}}{(k_2 \times k_3)_{\mathrm{d}}} \quad (9)$$

where $\varphi(t,1)_{\mathrm{r}}$ and $\varphi(t,2)_{\mathrm{d}}$ are the creep coefficient of a ring specimen (loaded at Day 1) and dog-bone specimen (loaded at Day 2), respectively. k_2 is a parameter accounting for the dimension and the concrete age in Equation (10) and k_3 accounts for the initial loading time (t_0) (Equation 11), as described in Australian Standard AS 3600[59]:

$$k_2 = \frac{\alpha_2 \times t^{0.8}}{t^{0.8} + 0.15 \times t_{\mathrm{h}}} \quad (10)$$

$$k_3 = \frac{2.7}{1 + \log(t_0)} \quad (11)$$

where $\alpha_2 = 1 + 1.12 \times e^{-0.008 \times t_{\mathrm{h}}}$ with t_{h} is the hypothetical thickness: $t_{\mathrm{h}} = \frac{2 \times A_{\mathrm{g}}}{u_{\mathrm{e}}}$. A_{g} and u_{e} are the cross-section area and exposed perimeter of the cross-section, respectively.

Figure 12 shows the correlation between the concrete tensile stress assessed experimentally ($\sigma_{\mathrm{c,act}}$) and the concrete tensile stress calculated using the analytical model ($\sigma_{\mathrm{c,analytical}}$) at the time of concrete cracking. The dotted line in Figure 12 represents the alignment between the experimental and analytical results. It can be observed that $\sigma_{\mathrm{c,analytical}}$ values are well-agreeing with $\sigma_{\mathrm{c,act}}$ values for all three LC3 concretes ($R^2 = 0.96$). The experimental concrete tensile stress was higher in LC3-CC1-44 while it was slightly lower than the analytical concrete tensile stress for LC3-CC2-30 and LC3-CC2-44 concretes. These results indicate that the analytical model outlined in Equation (6) can effectively predict the concrete tensile stress in the concrete restrained rings, thereby allowing to assess the risk of early-age cracking in LC3 concretes based on the free total shrinkage without carrying out the restrained ring test. This can be achieved thanks to the inclusion of the stress relaxation through the tensile creep and the aging coefficient in the equations. In addition, this analytical model can be considered as a predictive tool for other applications, for example, different cracking time due to different degree of restraint as proposed in a previous study by the authors.[25]

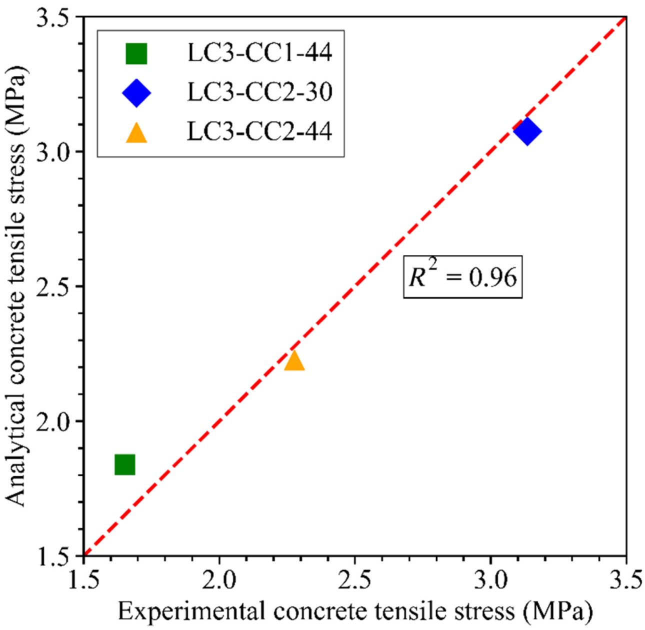

FIGURE 12 The comparison between concrete tensile stress assessed experimentally and the tensile stress calculated by the analytical model at concrete cracking. CC1, calcined clay 1; CC2, calcined clay 2; LC3, limestone calcined clay cement.

4.5 | Effect of calcined clay reactivity on the risk of early-age concrete cracking

Figure 13 shows the correlation between the instantaneous stress rate at cracking and the net time to cracking for both Ref and LC3 concretes. The net time to cracking was determined as the difference in days between the age of concrete at cracking and the age when drying was initiated. In addition, the classifications of potential for cracking including low, moderate-low,

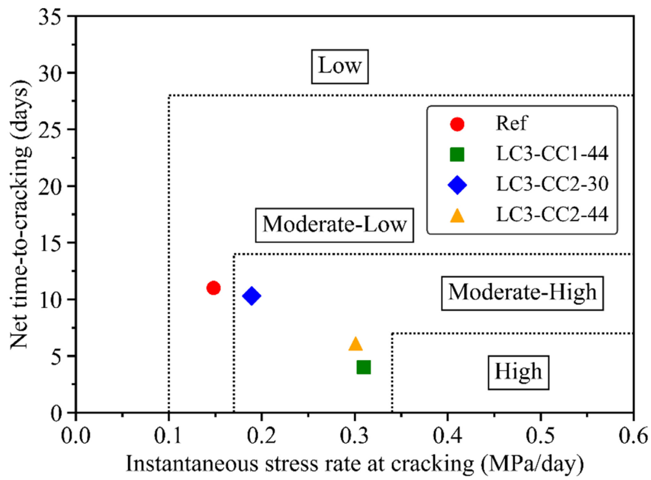

FIGURE 13 Correlation between instantaneous stress rate at cracking and net time to crack. CC1, calcined clay 1; CC2, calcined clay 2; LC3, limestone calcined clay cement.

moderate-high, and high based on ASTM C1581[47] are integrated in Figure 12. The Ref concrete was classified in the moderate-low category while all LC3 concretes were in moderate-high category. However, the difference between Ref and LC3-CC2-30 concrete in terms of instantaneous stress rate and net time to cracking was less than 10%, indicating that Ref and LC3-CC-30 concretes had a similar potential for cracking. On the other hand, LC3-CC1-44 and LC3-CC2-44 concretes had higher instantaneous stress rate at cracking and lower net time to cracking, implying a higher potential for cracking compared to Ref and LC3-CC2-30 concretes. These findings can be attributed to the variations in calcined clay reactivity (in Section 2.1) and binder replacement rates, resulting in distinct mechanical and viscoelastic properties among the LC3 concretes.

To provide more insights regarding the impacts of calcined clay reactivity (%), that is, amorphous content (%) and binder replacement rate on the risk of early-age cracking of LC3 concretes, the apparent calcined clay reactivity was calculated as follows:

$$\text{Apparent calcined clay reactivity}\left(R_{\text{app}}\right) = \frac{\text{Calcined clay reactivity}(\%) \times m_{\text{calcined clay}}}{m_{\text{binder}}} \quad (12)$$

where $m_{\text{calcined clay}}$ and m_{binder} are the mass (kg) of calcined clay and binder in the concrete mix as shown in Table 3. The apparent calcined clay reactivity of the three LC3 concretes is presented in Table 4. LC3-CC1-44 concrete exhibited the highest R_{app} value of 23.7 wt.% due to the high reactivity of CC1 (79 wt.% of amorphous phase) and high proportion of CC1 in the concrete mix. With the same replacement rate, the apparent calcined clay reactivity of LC3-CC2-44 was only 15.6 wt.% compared to 23.7 wt.% of LC3-CC1-44 due to the low reactivity of CC2 at 51 wt.% of amorphous phase. The R_{app} value of LC3-CC2-30 concrete was the lowest at 10.2 wt.% (Table 4).

The correlations between the apparent calcined clay reactivity (R_{app}) and the mechanical properties (compressive strength, indirect tensile strength, and elastic modulus) of LC3 concretes from Day 1 to Day 28 are shown in Figure 14. The average coefficients of

TABLE 4 Apparent calcined clay reactivity of LC3 concretes.

Concrete mixes	Apparent calcined clay reactivity wt.% (R_{app})
LC3-CC1-44	23.7
LC3-CC2-30	10.2
LC3-CC2-44	15.6

Abbreviations: CC1, calcined clay 1; CC2, calcined clay 2; LC3, limestone calcined clay cement.

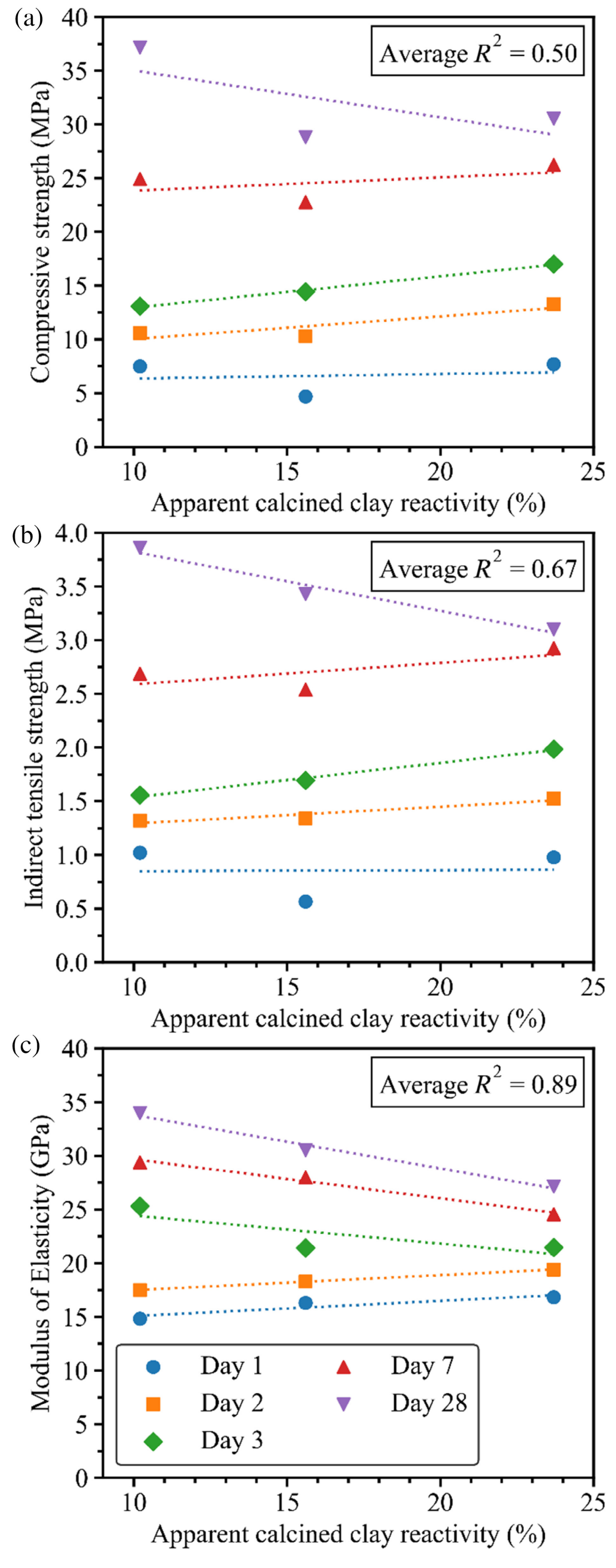

FIGURE 14 Correlations between apparent calcined clay reactivity and mechanical properties: (a) compressive strength, (b) indirect tensile strength, and (c) Modulus of elasticity.

determination (R^2) are also provided. The apparent calcined clay reactivity presented poor correlations with the compressive strength (Figure 14a) and the indirect tensile strength (Figure 14b), with average R^2 values only 0.50 and 0.67, respectively. Lee et al.[60] also reported a weak correlation between the compressive strength, tensile strength and the cracking time of restrained concrete rings using dune sand and crushed sand. A better correlation was observed between the apparent calcined clay reactivity and the modulus of elasticity (Figure 14c), with an average R^2 value of 0.89. Noticeably, the correlations displayed opposite trends between early days (less than 7 days after casting) and later days (28 days). In the early days, compressive strength, indirect tensile strength, and modulus of elasticity increased with the increase in apparent calcined clay reactivity, indicating the influence of rapid pozzolanic reaction of calcined clays on the development of the mechanical properties. However, at 28 days, the mechanical properties were primarily governed by GP cement hydration, and the highest values were observed in LC3-CC2-30, which had the highest percentage of GP cement in the concrete mix. The better mechanical properties of LC3-CC2-44 concrete compared to LC3-CC1-44 can be attributed to the lower calcined clay reactivity of CC2 which facilitated the hydration of the ternary binder. Cardinaud et al.[61] also reported that LC3 blends with low kaolinite content clay presented higher pozzolanic reactivity than LC3 with a higher metakaolin content. Both compressive strength and indirect tensile strength presented an increasing trend with the increase of R_{app} from Day 1 to Day 7 but a decreasing trend with the increase of R_{app} at 28 days. By contrast, the modulus of elasticity exhibited an upward trend at Day 1 and Day 2 while showing a downward trend from Day 3 to Day 28. This suggests that GP cement content governed the elastic modulus of LC3 concretes earlier than for the compressive strength and the indirect tensile strength. In general, the apparent calcined clay reactivity R_{app} cannot accurately be used to predict the mechanical properties of LC3 concretes.

Figure 15 illustrates the correlations between the apparent calcined clay reactivity and the total shrinkage measured using the concrete prisms and the unrestrained concrete rings. The apparent calcined clay reactivity and the prism total shrinkage in Figure 15a exhibited a poor correlation with the average R^2 value of 0.61. When increasing the apparent calcined clay reactivity higher than 15.6 wt.% in LC3-CC1-44 concrete, the total concrete shrinkage significantly increased. The R_{app} very poorly correlated with the total shrinkage of the unrestrained concrete rings (average $R^2 = 0.28$). The correlation trend was similar to that of the prism total shrinkage, except for the shrinkage at cracking. The total shrinkage values of the unrestrained rings showed an opposite trend at the time of concrete cracking of the corresponding restrained concrete rings. It can be attributed to the significant difference in cracking time between the LC3 concretes with low and high R_{app} value. Specifically, LC3-CC2-30 ($R_{app} = 10.2$ wt.%) and LC3-CC1-44 ($R_{app} = 23.7$ wt.%) cracked at 11.3 days and 5 days, respectively. As a result, LC3-CC2-30 concrete, which cracked at 11.3 days, developed more shrinkage than LC3-CC1-44 concrete, which cracked at 5 days. Overall, similar to mechanical properties, R_{app} is not suitable to assess LC3 concrete shrinkage.

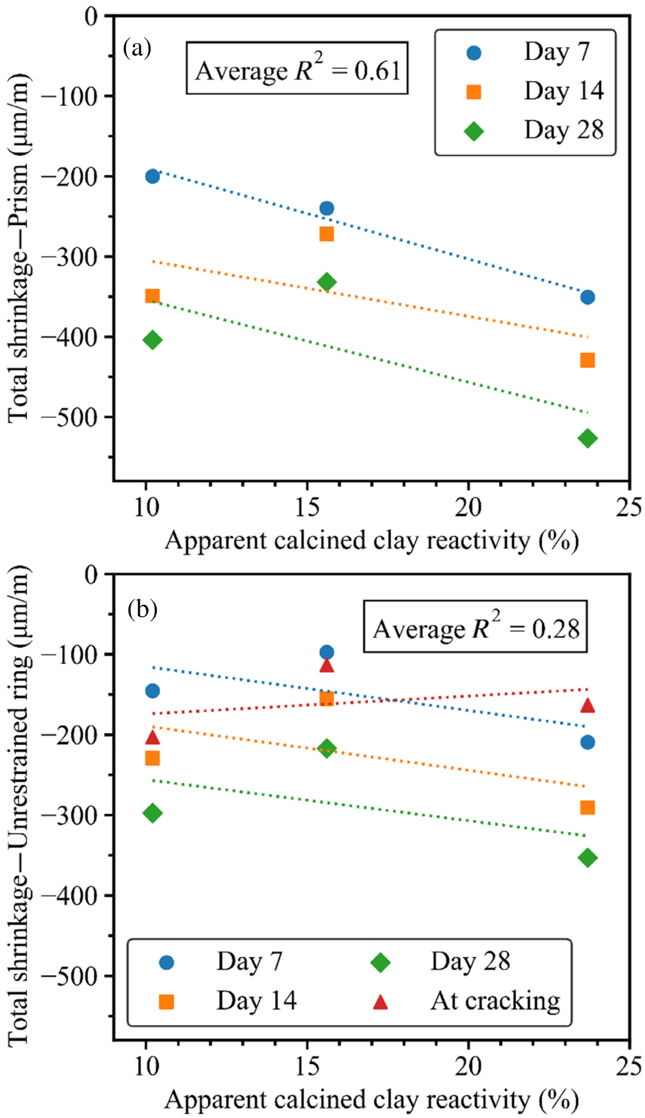

FIGURE 15 Correlations between apparent calcined clay reactivity and total shrinkage: (a) concrete prisms and (b) unrestrained concrete rings.

To gain further insights into the properties at the time of concrete cracking, Figure 16 presents the correlation between the apparent calcined clay reactivity R_{app} and the cracking time (a), the concrete tensile stress $\sigma_{c,act}$ (b), the instantaneous stress rate S (c), the tensile creep coefficient φ, and (d) at the time of concrete cracking. Except for instantaneous stress rate, S (Figure 16c), the apparent calcined clay activity R_{app} exhibited excellent correlations with time to cracking, concrete tensile stress, and tensile creep coefficient at concrete cracking, with R^2 values exceeding 0.96. Noticeably, the correlation between R_{app} and cracking time showed the highest R^2 value of 0.98, indicating that R_{app} could potentially be used as an indicator of LC3 concrete cracking time, that is, the cracking potential in LC3 concretes. Specifically, an increase in the apparent calcined clay reactivity led to a higher risk of early-age cracking in LC3 concretes. The correlation between the apparent calcined clay reactivity and the cracking time could be linked to the tensile creep of LC3 concrete. Lower R_{app} value resulted in higher LC3 concrete tensile creep coefficient at cracking (Figure 16d). For instance, LC3-CC2-30 concrete with $R_{app} = 10.2$ wt.% had the tensile creep coefficient (φ) of 1.6 at cracking, which was approximately twice the φ value of 0.8 in LC3-CC2-44 ($R_{app} = 23.7$ wt.%). As mentioned earlier in Section 4.3, higher tensile creep produces better relaxation effects on concrete tensile stress delaying the occurrence of concrete cracking.[56] Ston and Scrivener[32] revealed that LC3 blend had lower basic compression creep coefficients than OPC paste but no drying or total creep was reported. The lower basic creep coefficients are attributed to the higher viscosity and different porosity of C-S-H in LC3 compared to OPC paste.[32] In this study, the total tensile creep of concrete, including tensile basic creep and tensile drying creep, was measured, showing that the tensile creep coefficient of LC3 concretes is higher than that of plain GP cement concrete. By contrast, Stone and Scrivener[32] assessed the compressive creep of LC3 pastes, leading to opposite conclusions. Different values of compression and tensile creep coefficients measured on the same concrete were reported by previous studies.[62–64] For instance, Huang et al.[62] reported a higher tensile creep compared to compressive creep for fly ash concretes loaded at the same age. As shown in Figure 16b, the concrete tensile stress $\sigma_{c,act}$ decreased with the increase in apparent calcined clay reactivity, which is consistent with the correlation with time to cracking (Figure 16a). In other words, a longer cracking time allowed higher concrete tensile stress $\sigma_{c,act}$ to develop in LC3 concretes, thereby producing similar trends in Figure 16a,b. On the other hand, an increase of R_{app} decreased the instantaneous stress rate S at cracking in Figure 16c, with a R^2 of 0.71 in the correlation. This can be attributed to the higher strain development in LC3-CC1-44 ($R_{app} = 23.7$ wt.%) due to a higher shrinkage

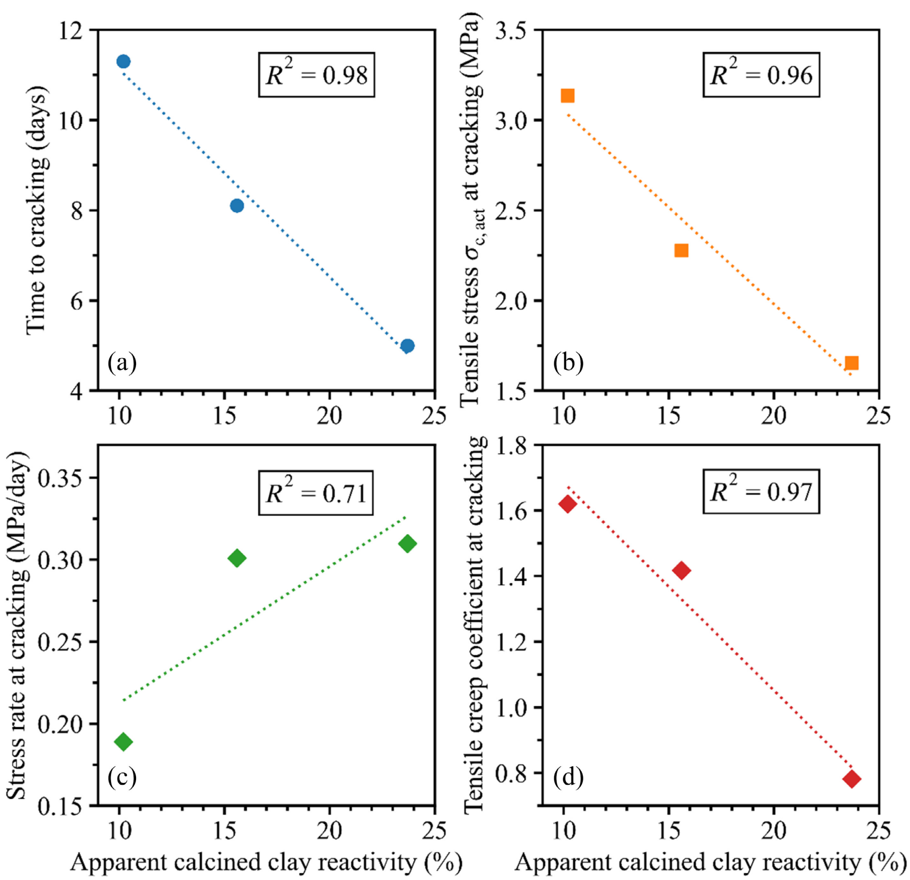

FIGURE 16 Correlations of apparent calcined clay reactivity and (a) Time to cracking, (b) Concrete tensile stress at cracking, (c) instantaneous stress rate at cracking, and (d) tensile creep coefficient at cracking.

and a lower tensile creep coefficient than the other LC3 concretes. The relationships described in this paper are based on only three LC3 concretes. As a result, further studies are required to better understand the correlations between the apparent calcined clay reactivity (R_{app}) and the properties related to the early-age cracking potential of LC3 concretes.

5 | CONCLUSION

This study investigates the influence of the calcined clay reactivity on the risk of restrained shrinkage-induced early-age cracking in LC3 concretes. Mechanical properties, time to cracking, tensile creep coefficient, total shrinkage, and tensile stress development were evaluated. Two types of calcined clay with significantly different reactivity and two different replacement rates were considered. The results were compared with a plain GP cement concrete and blended concretes incorporating fly ash or GGBFS. The main findings from this study are presented as follows:

- The high reactivity of the calcined clay CC1 resulted in a significantly higher concrete total shrinkage than that of calcined clay CC2 concretes, also resulting in the highest total shrinkage values among all reference concretes. The total shrinkage of the low reactivity calcined clay (CC2) concretes fell within the range of total shrinkage of the concretes containing fly ash and GGBFS. Noticeably, the LC3 concrete with 44 wt.% replacement rate with low reactivity calcined clay (LC3-CC2-44) showed a lower total shrinkage than that of reference concrete, demonstrating the significant impact of the calcined clay reactivity on the development of total shrinkage in LC3 concrete.
- The restrained concrete ring with high reactivity calcined clay (LC3-CC1-44) presented the shortest cracking time at 5 days. However, by using low reactivity calcined clay (CC2 instead of CC1), the cracking time increased significantly. The cracking time of LC3-CC2-30 concrete was comparable to the reference concrete at 11.5 days while LC3-CC2-44 exhibited a cracking time similar to concrete containing 40 or 60 wt.% GGBFS.
- LC3-CC1-44 and LC3-CC2-44 concretes showed higher tensile creep coefficients than that of reference concrete up to 10 days and 16 days, respectively. LC3-CC2-30 presented a higher tensile creep coefficient than that of reference concrete until 28 days. At the cracking time of the restrained concrete ring, the tensile creep coefficient of LC3-CC2-30 was approximately 48% higher than that of the Ref concrete. The higher creep coefficient can provide beneficial relaxation toward concrete tensile stress to delay concrete cracking.
- The analytical model, initially developed for GP cement, fly ash, and GGBFS, successfully predicted the development of the concrete tensile stress in the LC3 concrete restrained rings. This demonstrates that the analytical model can be applied to LC3 concretes, similarly to other traditional SCMs in concretes.
- According to ASTM C1581, LC3 concretes were classified as moderate-high category of early-age cracking. However, the instantaneous stress rate of LC3-CC2-30 was very close to that of the reference concrete, in the moderate-low category.
- In this study, an apparent calcined clay reactivity coefficient (R_{app}) was proposed accounting for both reactivity of calcined clay and replacement rate in the binder. R_{app} exhibited an excellent correlation with the cracking time of the restrained LC3 concrete rings. Furthermore, the correlation between R_{app} and both concrete tensile stress and creep coefficient at cracking time was also excellent, although R_{app} did not correlate well with the development of the mechanical properties of LC3 concretes. The R_{app} coefficient could potentially be used in practice to assess the early-age cracking potential of LC3 concretes, allowing to reduce the risk of restrained shrinkage-induced cracking of LC3 concrete structures by selecting appropriate calcined clays and mix design for specific high-risk applications.

ACKNOWLEDGMENTS

This research was funded by Cement Concrete Aggregate Australia (CCAA) and ARC Linkage project LP170100912 titled "Shrinkage, cracking, self-healing and corrosion in blended cement concrete". The authors would like to thank the School of Civil and Environmental Engineering, University of Technology Sydney, for UTS Tech Lab facilities and support. Open access publishing facilitated by University of Technology Sydney, as part of the Wiley - University of Technology Sydney agreement via the Council of Australian University Librarians.

CONFLICT OF INTEREST STATEMENT

The authors declare that they have no known competing financial interests or personal relationships that could have appeared to influence the work reported in this paper.

DATA AVAILABILITY STATEMENT

The data that support the findings of this study are available from the corresponding author upon reasonable request.

ORCID

Quang Dieu Nguyen https://orcid.org/0000-0002-0213-6652

REFERENCES

1. Watari T, Cao Z, Hata S, Nansai K. Efficient use of cement and concrete to reduce reliance on supply-side technologies for net-zero emissions. Nat Commun. 2022;13:4158.
2. Bataille C, Nilsson LJ, Jotzo F. Industry in a net-zero emissions world: new mitigation pathways, new supply chains, modelling needs and policy implications. Energy Clim Change. 2021;2:100059.
3. Scrivener KL, John VM, Gartner EM. Eco-efficient cements: potential economically viable solutions for a low-CO_2 cement-based materials industry. Cem Concr Res. 2018;114:2–26.
4. Madlool NA, Saidur R, Hossain MS, Rahim NA. A critical review on energy use and savings in the cement industries. Renew Sustain Energy Rev. 2011;15:2042–60.
5. Favier A, De Wolf C, Scrivener K, Habert G. A sustainable future for the European cement and concrete industry: technology assessment for full decarbonisation of the industry by 2050. Zurich: ETH Zurich; 2018.
6. Damtoft JS, Lukasik J, Herfort D, Sorrentino D, Gartner EM. Sustainable development and climate change initiatives. Cem Concr Res. 2008;38:115–27.
7. Snellings R, Mertens G, Elsen J. Supplementary cementitious materials. Rev Mineral Geochem. 2012;74:211–78.
8. Lothenbach B, Scrivener K, Hooton RD. Supplementary cementitious materials. Cem Concr Res. 2011;41:1244–56.
9. Juenger MCG, Snellings R, Bernal SA. Supplementary cementitious materials: new sources, characterization, and performance insights. Cem Concr Res. 2019;122:257–73.
10. Kermeli K, Edelenbosch OY, Crijns-Graus W, van Ruijven BJ, Mima S, van Vuuren DP, et al. The scope for better industry representation in long-term energy models: modeling the cement industry. Appl Energy. 2019;240:964–85.
11. Nidheesh PV, Kumar MS. An overview of environmental sustainability in cement and steel production. J Clean Prod. 2019;231:856–71.
12. Zunino F, Martirena F, Scrivener K. Limestone calcined clay cements (LC3). ACI Mater J. 2021;118:49–60.
13. Scrivener K, Martirena F, Bishnoi S, Maity S. Calcined clay limestone cements (LC3). Cem Concr Res. 2018;114:49–56.
14. Joseph S, Dhandapani Y, Geddes DA, Zhao Z, Bishnoi S, Vieira M, et al. Mechanical properties of concrete made with calcined clay: a review by RILEM TC-282 CCL. Mater Struct. 2023;56:84.
15. Mishra G, Emmanuel AC, Bishnoi S. Influence of temperature on hydration and microstructure properties of limestone-calcined clay blended cement. Mater Struct. 2019;52:91.
16. Dhandapani Y, Joseph S, Bishnoi S, Kunther W, Kanavaris F, Kim T, et al. Durability performance of binary and ternary blended cementitious systems with calcined clay: a RILEM TC 282 CCL review. Mater Struct. 2022;55:145.
17. Nguyen QD, Khan MSH, Castel A. Engineering properties of limestone calcined clay concrete. J Adv Concr Technol. 2018;16:343–57.
18. Nguyen QD, Khan MSH, Castel A. Chloride diffusion in limestone flash calcined clay cement concrete. ACI Mater J. 2020;117:165–75.
19. Khan MSH, Nguyen QD, Castel A. Performance of limestone calcined clay blended cement-based concrete against carbonation. Adv Cement Res. 2020;32:481–91.
20. Shi Z, Ferreiro S, Lothenbach B, Geiker MR, Kunther W, Kaufmann J, et al. Sulfate resistance of calcined clay – limestone – Portland cements. Cem Concr Res. 2019;116:238–51.
21. Nguyen QD, Kim T, Castel A. Mitigation of alkali-silica reaction by limestone calcined clay cement (LC3). Cem Concr Res. 2020;137:106176.
22. Nguyen QD, Afroz S, Zhang Y, Kim T, Li W, Castel A. Autogenous and total shrinkage of limestone calcined clay cement (LC3) concretes. Constr Build Mater. 2022;314:125720.
23. Hossain AB, Weiss J. Assessing residual stress development and stress relaxation in restrained concrete ring specimens. Cement Concr Comp. 2004;26:531–40.
24. Rodriguez J, Ortega L, Casal J, Diez J. Corrosion of reinforcement and service life of concrete structures. In: Sjostrom C, editor. Durability of building materials and components. Volume 7. London: Routledge; 2018. p. 117–26.
25. Zhang Y, Afroz S, Nguyen QD, Kim T, Eisenträger J, Castel A, et al. Analytical model predicting the concrete tensile stress development in the restrained shrinkage ring test. Constr Build Mater. 2021;307:124930.
26. Chen P, Zheng W, Zhou X. Creep of reinforced high-strength concrete-containing industrial by-products silica fume and slag. Struct Concr. 2021;22:E549–62.
27. Miltenberger MA, Attiogbe EK, See HT. Potential for restrained shrinkage cracking of concrete and mortar. Cement Concr Aggregates. 2004;26:1–8.
28. See HT, Attiogbe EK, Miltenberger MA. Shrinkage cracking characteristics of concrete using ring specimens. Aci Mater J. 2003;100:239–45.
29. Altoubat S, Talha Junaid M, Leblouba M, Badran D. Effectiveness of fly ash on the restrained shrinkage cracking resistance of self-compacting concrete. Cement Concr Compos. 2017;79:9–20.
30. Akkaya Y, Ouyang C, Shah SP. Effect of supplementary cementitious materials on shrinkage and crack development in concrete. Cement Concr Compos. 2007;29:117–23.
31. Afroz S, Nguyen QD, Zhang Y, Kim T, Castel A. Evaluation of cracking potential parameters for low to high grade concrete with fly ash or slag. Constr Build Mater. 2022;350:128891.
32. Ston J, Scrivener K. Basic creep of limestone–calcined clay cements: an experimental and numerical approach. Theor Appl Fract Mech. 2019;103:102270.
33. Scrivener K, Avet F, Maraghechi H, Zunino F, Ston J, Hanpongpun W, et al. Impacting factors and properties of limestone calcined clay cements (LC3). Green Mater. 2019;7:3–14.
34. Afroz S, Zhang Y, Nguyen QD, Kim T, Castel A. Shrinkage of blended cement concrete with fly ash or limestone calcined clay. Mater Struct. 2023;56:15.
35. Du H, Pang SD. High-performance concrete incorporating calcined kaolin clay and limestone as cement substitute. Constr Build Mater. 2020;264:120152.
36. Dhandapani Y, Sakthivel T, Santhanam M, Gettu R, Pillai RG. Mechanical properties and durability performance of concretes with limestone calcined clay cement (LC3). Cem Concr Res. 2018;107:136–51.
37. Afroz S, Nguyen QD, Zhang Y, Kim T, Castel A. Cracking of limestone calcined clay blended concrete and mortar under restrained shrinkage. Constr Build Mater. 2023;386:131599.

38. Nguyen QD, Afroz S, Castel A. Influence of calcined clay reactivity on the mechanical properties and chloride diffusion resistance of limestone calcined clay cement (LC3) concrete. J Mar Sci Eng. 2020;8:301.
39. Rietveld HM. A profile refinement method for nuclear and magnetic structures. J Appl Cryst. 1969;2:65–71.
40. AS, AS 3972. General purpose and blended cements. Sydney, NSW: Standards Australia; 2010.
41. C595/C595M − 21. Standard specification for blended hydraulic cements. West Conshohocken, PA: ASTM International; 2021.
42. ASTM C192/C192M. 16a: standard practice for making and curing concrete test specimens in the laboratory. West Conshohocken, PA: ASTM International; 2016.
43. AS 1012.8.4. Method for making and curing concrete - drying shrinkage specimens prepared in the field or in the laboratory. Sydney, NSW: Standards Australia; 2015.
44. ASTM, ASTM C469/C469M-14. Standard test method for static modulus of elasticity and Poisson's ratio of concrete in compression. West Conshohocken, PA: ASTM International; 2014.
45. ASTM, ASTM C496/C496M-17. Standard test method for splitting tensile strength of cylindrical concrete specimens. West Conshohocken, PA: ASTM International; 2017.
46. AS, AS 1012.13. Methods of testing concrete: determination of the drying shrinkage of concrete for samples prepared in the field or in the laboratory. Sydney, NSW: Standards Australia; 2015.
47. ASTM, ASTM C1581/C1581M-18a. Standard test method for determining age at cracking and induced tensile stress characteristics of mortar and concrete under restrained shrinkage. West Conshohocken, PA: ASTM International; 2018.
48. Zhang Y, Afroz S, Nguyen QD, Kim T, Castel A, Xu T. Modeling blended cement concrete tensile creep for standard ring test application. Struct Concr. 2023;24:2170–88.
49. Nguyen QD, Khan MSH, Xu TF, Castel A. Mitigating the risk of early age cracking in Fly ash blended cement-based concrete using ferronickel slag sand. J Adv Concrete Technol. 2019;17: 295–308.
50. Khan I, Castel A, Gilbert RI. Tensile creep and early-age concrete cracking due to restrained shrinkage. Constr Build Mater. 2017;149:705–15.
51. Antoni M, Rossen J, Martirena F, Scrivener K. Cement substitution by a combination of metakaolin and limestone. Cem Concr Res. 2012;42:1579–89.
52. Li Z, Liu J, Ye G. Drying shrinkage of alkali-activated slag and fly ash concrete; a comparative study with ordinary portland cement concrete. Heron. 2019;64:1–15.
53. Afroz S, Kim T, Castel A. Distinct effect of hydration of calcined kaolinitic clay–limestone blended cement on microstructure and autogenous shrinkage. J Mater Civ Eng. 2023;35: 04023481.
54. Khan I, Xu T, Khan MSH, Castel A, Gilbert RI. Effect of various supplementary cementitious materials on early-age concrete cracking. J Mater Civ Eng. 2020;32:04020049.
55. Pane I, Hansen W. Early age creep and stress relaxation of concrete containing blended cements. Mater Struct. 2002;35:92–6.
56. Gilbert RI, Ranzi G. Time-dependent behaviour of concrete structures. London: CRC Press; 2010.
57. Li Z, Delsaute B, Lu T, Kostiuchenko A, Staquet S, Ye G. A comparative study on the mechanical properties, autogenous shrinkage and cracking proneness of alkali-activated concrete and ordinary Portland cement concrete. Constr Build Mater. 2021;292:123418.
58. Zdenek B. Prediction of concrete creep effects using age-adjusted effective modulus method. ACI J Proc. 1972;69:212–7.
59. AS, AS 3600. Concrete structures. Sydney, NSW: Standards Australia; 2018.
60. Lee E, Park S, Kim Y. Drying shrinkage cracking of concrete using dune sand and crushed sand. Constr Build Mater. 2016; 126:517–26.
61. Cardinaud G, Rozière E, Martinage O, Loukili A, Barnes-Davin L, Paris M, et al. Calcined clay – limestone cements: hydration processes with high and low-grade kaolinite clays. Constr Build Mater. 2021;277:122271.
62. Huang Y, Xie T, Ding Y, Fei D, Ding S. Comparison of tensile and compressive creep of hydraulic concrete considering loading/unloading under unified test conditions. Constr Build Mater. 2021;286:122763.
63. Rossi P, Tailhan J-L, Le Maou F. Comparison of concrete creep in tension and in compression: influence of concrete age at loading and drying conditions. Cem Concr Res. 2013;51:78–84.
64. Ranaivomanana N, Multon S, Turatsinze A. Tensile, compressive and flexural basic creep of concrete at different stress levels. Cem Concr Res. 2013;52:1–10.

AUTHOR BIOGRAPHIES

Emily Canda, PhD Candidate, School of Civil and Environmental Engineering, University of Technology Sydney (UTS), Sydney, NSW 2007, Australia.

Quang Dieu Nguyen, Postdoctoral Research Fellow, School of Civil and Environmental Engineering, University of Technology Sydney (UTS), Sydney, NSW 2007, Australia.

Rackel San Nicolas, Senior Lecturer, Department of Infrastructure Engineering, University of Melbourne (UoM), Melbourne, VIC 3010, Australia.

Haleh Rasekh, Senior Lecturer, School of Civil and Environmental Engineering, University of Technology Sydney (UTS), Sydney, NSW 2007, Australia.

Arnaud Castel, Professor, School of Civil and Environmental Engineering, University of Technology Sydney (UTS), Sydney, NSW 2007, Australia.

How to cite this article: Canda E, Nguyen QD, San Nicolas R, Rasekh H, Castel A. Effect of calcined clay reactivity on the risk of restrained shrinkage-induced early-age concrete cracking. Structural Concrete. 2025;26(2):1892–910. https://doi.org/10.1002/suco.202301131